NJC

Accepted Manuscript

This article can be cited before page numbers have been issued, to do this please use: S. Rayati, P. Nafarieh and M. M. Amini, *New J. Chem.*, 2018, DOI: 10.1039/C8NJ00743H.

ROYAL SOCIETY OF CHEMISTRY

rsc.li/njc

DOI: 10.1039/C8NJ00743H

Journal Name

ARTICLE

Synthesis, characterization and catalytic application of manganese porphyrins bonded to the novel modified SBA-15

Received 00th January 20xx,
Accepted 00th January 20xx

DOI: 10.1039/x0xx00000x

www.rsc.org/

Saeed Rayati,*[a] Parinaz Nafarieh [a] and Mostafa M. Amini [b]

In the present research, a highly ordered mesoporous silica material (SBA-15) was functionalized with imidazole as a functionalizing reagent (SBA-TMSIm) and then characterized by FT-IR spectroscopy, thermogravimetric analysis (TGA), powder X-ray diffraction (XRD) and nitrogen adsorption/desorption isotherm. The SBA-TMSIm was used as a support for coordinative anchoring of tetraphenylporphyrinato-manganese(III) acetate [Mn(TPP)OAc] via axial ligation. The prepared catalyst was characterized by different spectroscopic methods and the amount of loaded metalloporphyrin on SBA-TMSIm was determined by atomic absorption spectroscopy. Finally, the immobilized metalloporphyrin was found to be an efficient catalyst in the oxidation of styrene with molecular oxygen and isobutyraldehyde (IBA) as the co-oxidant. In addition to that, this aerobic oxidation system was used to oxidize various olefins and the results showed their epoxide was the major products.

Introduction

In the past few decades, the use of toxic and harmful oxidants in the oxidation reactions would dramatically decrease the qualification of systems from environmental-friendly approaches. Among of the different sources of oxygen, use of non-polluting oxygen donors, such as molecular oxygen in hydrocarbon biomimetic oxygenation, is of particular interest.[1-4] One of the most important challenges is the activation process of molecular O_2 with transition metal complexes to perform a number of reactions including the highly selective oxidation of different substrates. A number of first-row transition metals ions (such as Mn, Fe, Cu) which are employed by metalloenzymes are capable of activating molecular O_2.[5]

Manganese porphyrins have been extensively used as efficient catalysts for oxidation of alkenes with molecular O_2 as a green oxidant.[6-8] Early works demonstrated that simple biomimetic metalloporphyrins can bind much easier to O_2 in the presence of donor bases coordinated through the axial site as a mimicking of proximal histidine nitrogen bonding structure for hemoglobin and myoglobin anchored in a cleft in the globin chain.[9,10] On the other hand, axial base assists the molecular oxygen via π-donation to coordinate more readily to the metal center, which leads to significant increase in the aerobic oxidation yield. The basicity of the proximal ligand is also a determining factor in dioxygen complex formation. It has studied that in manganese-porphyrins the strong π-donor imidazole is the best nitrogen donor among the others, which would increase the oxygen-metal affinity.[11-13] Axial bases can directly add to the reaction atmosphere or it may attach to the metal center from the first place.

Metalloporphyrins can partially decompose during the catalytic process. Therefore, immobilization of metalloporphyrins onto solid organic and inorganic supports is a well-structured way to bridge the gap between heterogeneous and homogeneous catalytic systems. Heterogeneous phases are preferred with clarity due to their advantages of stability in reaction phase against temperature and pressure changes and the ability to separate from reaction solution for later use.[6] However, the system efficiency slightly decreases because of not being able to achieve all of the active sites of the catalyst.[14,15] Modifying solid supports with donor groups can significantly improve the catalytic properties in comparison with non-modified supports due to the combination of two different catalytic sites in one material. Recent works on some supports from bulk to nano modified by groups such as pyridine and imidazole have been performed.[16,17]

Santa Barbara Amorphous (SBA-15) is a special type of ordered mesoporous silica support with unique and significant properties of the large pore size, thick pore walls (4-6 nm), thermal and mechanical stability, highly ordered mesostructured, large specific surface area (700-1000 m2/g) and easy synthesis, which make it a beneficial catalyst support

[a] Department of Chemistry, K.N. Toosi University of Technology, P.O. Box 16315-1618, Tehran 15418, Iran. E-mail: rayati@kntu.ac.ir, srayati@yahoo.com; Fax: +98 21 22853650; Tel: +98 21 22850266
[b] Department of Chemistry, Shahid Beheshti University, G.C., Tehran 1983963113, Iran

† Footnotes relating to the title and/or authors should appear here.
Electronic Supplementary Information (ESI) available: [details of any supplementary information available should be included here]. See DOI: 10.1039/x0xx00000x

View Article Online
DOI: 10.1039/C8NJ00743H

for wide applications.[18-20] In spite of favourable functions of SBA-15 in catalysis, it would be requested to modify SBA-15 to enhance and optimize its catalytic activity by supporting or immobilizing on other elements or complement other catalyst, especially for thermal toleration and reusability. In addition, SBA-15 is one of the best materials to be modified and functionalized because it has a controllable pore size, pore volume and high surface area. A study of functionalizing SBA-15 with various groups such as sulfonic, amino propyl, imidazole, triazole group has investigated recently.[21-23] The combination of the SBA-15 with terminal imidazole group enables a good chance to design and synthesize novel supported metalloporphyrins to mimic the function of P-450 enzymes, and simultaneously reach the desirable features of heterogeneous systems.

In this perspective, first imidazole reagent [5-((3-(trimethoxysilyl)propyl)carbamoyl)-1H-imidazole-4-carboxylic acid] (TMSIm) was prepared as the SBA-15 functionalizing agent. Then the [SBA-TMSIm] modified support were synthesized and characterized and was utilized as a support for [Mn(TPP)OAc] for the oxidation of styrene and various olefins in isobutyraldehyde/O_2 system.

Experimental

Instruments and reagents

Chemicals were purchased from Merck or Fluka and used without further purification. The UV-Vis spectra were recorded on a PerkinElmer Lambda 25 UV-Vis spectrophotometer. The solid samples were identified by X-ray powder diffraction (XRD) using a STOE diffractometer with Cu-K_α radiation (λ = 0.15418 nm) at 40 kV and 40 mA. The diffraction patterns were recorded in the Bragg angle (2θ) range from 0.5° to 10° for small angle XRD with a position sensitive detector using a step size of 0.06°. Infrared spectra were recorded (KBr pellets) on an ABB Bomem: FTLA 2000-100 in the 400 to 4000 cm^{-1} range. Thermogravimetry and differential thermal analysis (TGA/DTGA) were carried out on a Mettler Toledo (TGA/DTGA) under N_2 atmosphere at a heating rate of 10 °C min^{-1}. The manganese content of catalyst was measured by atomic absorption spectroscope (model GVC932) with air-acetylene flame. Nitrogen adsorption-desorption measurements were carried out on a BELSORP-mini II at 77 K. The samples (36 mg) were previously degassed at 150 °C for 15 h. The specific surface area was determined by the adsorption isotherm with relative pressure 0.01 m^2/g using BET method. The pore size distribution was calculated by BJH method from the desorption isotherm, and the total pore volume was obtained at 0.35-200 nm in pore diameter. The micro pore volume, microporous surface area, and external surface area were obtained by the t-plot method. Gas chromatography (GC) analyses were conducted on an Agilent chromatograph (model 7890B) equipped with flame ionization detector (FID) and capillary column HP-5 (phenyl methyl siloxane 30 m × 0.32 mm × 0.25 μm).

Preparation of the heterogenized catalyst

Preparation of [H_2TPP], [Mn(TPP)OAc] and 5-((3-(trimethoxysilyl)propyl) carbamo- yl)-1H-imidazole-4-carboxylic acid (TMSIm) Meso-tetraphenylporphyrin [H_2TPP] was prepared according to the literature.[25] The [Mn(TPP)OAc] was prepared and characterized according to the already reported procedure for metalation of porphyrins.[26] For the synthesis of imidazole functionalizing reagent (TMSIm), in a 250 mL round-bottomed two-necked flask equipped with a magnetic stirrer and a condenser, 16 mmol (2.5 g) of 4,5-imidazoledicarboxylic acid were suspended in 100 mL of dry CH_2Cl_2 under N_2 atmosphere. A total of 5 mL of oxalyl chloride was slowly added from a dropping funnel. After 12 h, the solvent was removed under reduced pressure and the residue was suspended again in 100 mL of dry CH_2Cl_2. After the addition of 7 mL of triethylamine to the reaction mixture, 4.0 g of 3 aminopropyltrimethoxysilane was slowly added. The reaction mixture was stirred at room temperature for a further 4 h. The mixture was suspended in water for 1 h in order to remove the formed salts and any impurities. Then the organic phase was separated and the solvent was removed under reduced pressure to obtain brownish viscous oil. To avoid hydrolysis, 100 mL of dried toluene added to the product and kept in the fridge. The formation of the imidazole-functionalizing reagent confirmed by ^{1}H NMR spectroscopy. ^{1}H NMR ($CDCl_3$, ppm): 0.61 (t, 2H), 1.53 (m, 2H), 3.21 (t, 2H), 3.60 (s, 9H), 8.22 (s, 1H), 8.91 (s, 1H), 12.21 (s, 1H) and 12.98 (s, 1H).

Preparation of imidazole functionalized SBA-15 (SBA-TMSIm) To functionalize SBA-15 by imidazole, the general procedure was used. Briefly, SBA-15 (1.0 g) was suspended in 50 mL toluene, the mixture was stirred for 1 h, and then 2.0 g of TMSIm was added and refluxed for 24 h. The white solid was removed from the solvent by filtration, washed with toluene and ethanol, and then dried at room temperature. The formation of this nanoporous silica was confirmed by FT-IR spectroscopy, low angle X-ray powder diffraction (XRD) and thermal analysis.

Preparation of [Mn(TPP)OAc/SBA-TMSIm] [Mn(TPP)OAc] (0.10 g) and SBA-TMSIm mesoporous support (0.40 g) were added to 30 mL dichloromethane and mixed on a shaker for 30 minutes. The mixture was allowed to react at room temperature for 24 h. Then the solid was filtered and washed with dichloromethane and dried in air. FT-IR, XRD, BET, TGA/DTA, UV-Vis, and atomic absorption spectroscopy were used to characterize the resulting heterogenized catalyst. The schematic preparation route of the synthesized solid support is shown in scheme 1.

DOI: 10.1039/C8NJ00743H

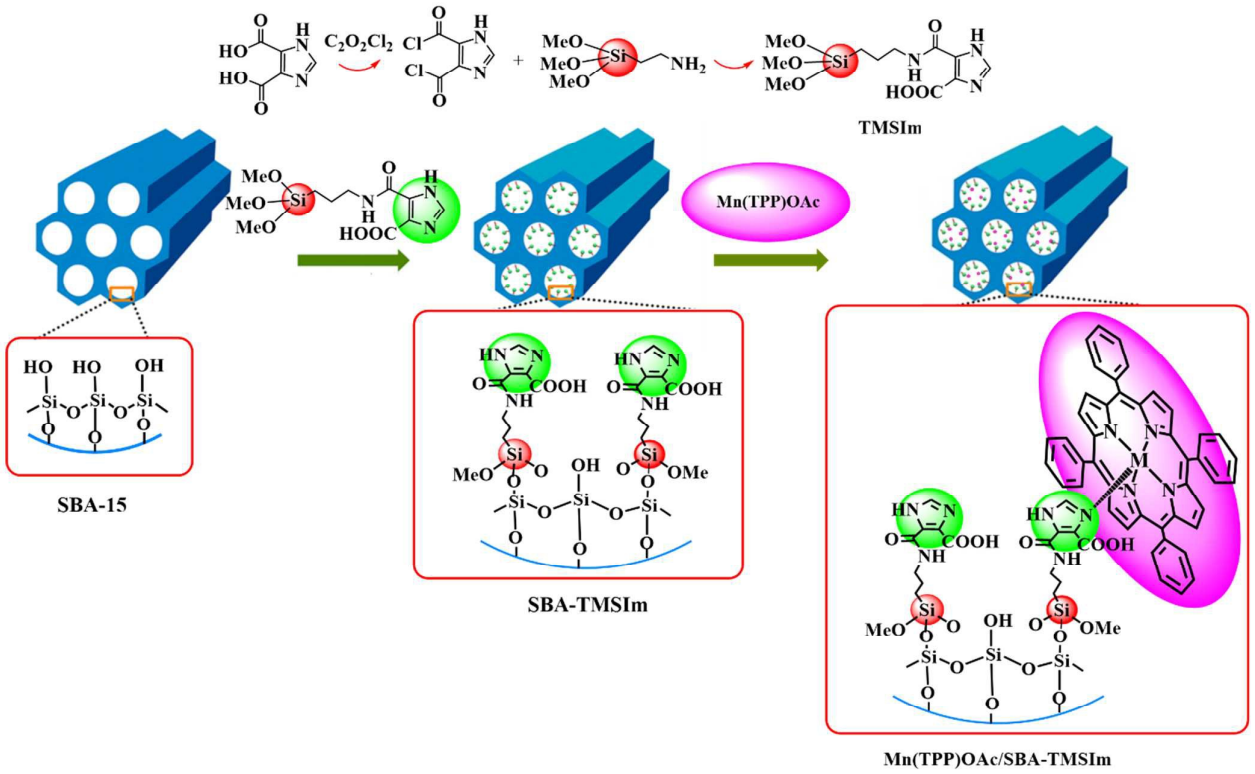

Scheme 1 Schematic synthesis of [Mn(TPP)OAc/SBA-TMSIm].

General heterogeneous oxidation procedure

Catalytic performance of [Mn(TPP)OAc/SBA-TMSIm] was carried out in a 5-mL test tube in a high temperature water bath keeping the temperature between 40-50 °C. In a typical procedure, to 1 mL of acetonitrile, 0.0021 mmol of prepared catalyst, 0.0189 mmol of substrate and 0.0567 mmol of isobutyraldehyde as a co-reagent were added. The mixture was stirred slowly by magnetic stirrer under oxygen atmosphere (pure oxygen gas balloon directly attached to the reaction system) for 1 h. After reaction completed, solid phase was separated by centrifugation and the products were characterized by GC.

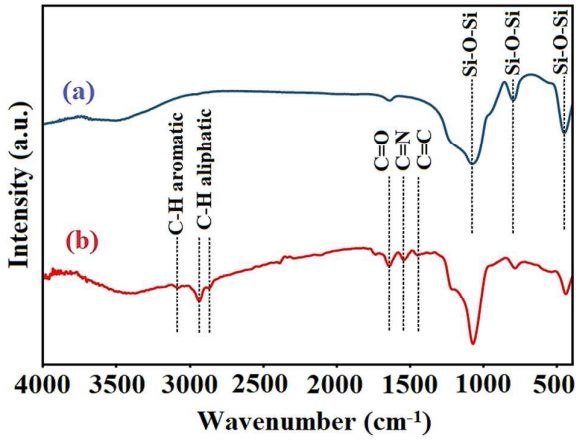

Figure 1 FTIR spectra of (a) SBA-15 and (b) [SBA-TMSIm].

Results and discussion

Characterization of imidazole functionalized SBA-15 (SBA-TMSIm)

FT-IR spectra. FT-IR spectrum of [SBA-TMSIm] in addition to the typical bands of mesoporous silica,[21,27-29] asymmetric and symmetric Si–O–Si characteristic stretching vibrations at 1076 and 800 cm^{-1} along with Si–OH at 950 cm^{-1} and Si–O–Si bending at 458 cm^{-1}, showed new bands at 3422, 2929, 1648, 1551 and 1420 cm^{-1}. These bands, which are corresponded to C–H aromatic, C–H aliphatic, C=O, C=N and C=C, respectively, confirmed 5-((3-(trimethoxysilyl)propyl)carbamoyl)-1H-imidazole-4-carboxylic acid groups' successfully immobilized into SBA-15 (Figure 1).[30]

X-ray diffraction. Low-angle XRD patterns of SBA-15 before and after imidazole-modified exhibit a single and strong diffraction peak at 2θ between 0.5 and 1.5° as seen in Figure 2, which can be indexed to the (100) hkl reflection, indicating the presence of a mesoporous structure. This reflection is associated with the P6mm hexagonal symmetry typical of SBA-15 material and

View Article Online
DOI: 10.1039/C8NJ00743H
ARTICLE Journal Name

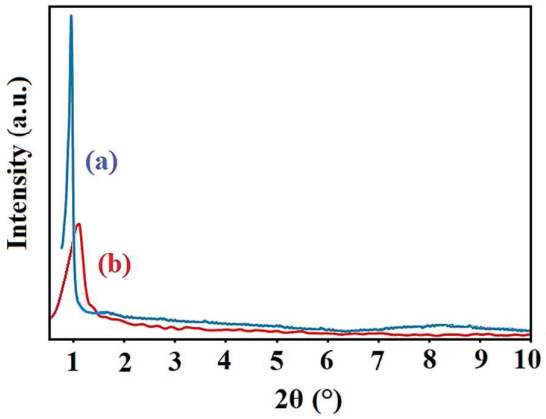

Figure 2 Low-angle XRD pattern of (a) SBA-15 and (b) [SBA-TMSIm].

indicating a significant degree of long-range ordering in the structure and a well-formed hexagonal lattice.[31] Due to the grafting of TMSIm groups, the diffraction peak of [SBA-TMSIm] shifted to a higher angle and became weaker compared with unmodified one. These results indicate that the mesoporous phase of the compound was maintained, while the integrity of the mesoporous structure was affected by the incorporation of TMSIm functionalizing agent.[32]

TGA/DTGA analysis. The thermal stability of [SBA-TMSIm] compound (Figure 3) was studied by TGA/DTGA analysis. The total weight loss was measured to be 10.3% during pyrolysis in N_2. The differential thermogravimetric analysis (DTGA) curve of [SBA-TMSIm] showed two distinct weights loss centered at 267 and 403 °C. The first one is attributed to the loss of free water molecules, which are accommodated in cylindrical pores, which are maintained in the pores up to the temperature higher than that applied in the sample preparation for sorption measurements.[33] These water molecules can release from 100 up to 200 °C, and in this DTGA curve, they seem to be released at 267 °C with 4.1% weight loss. A weight loss occurred between 200 and 800 °C which is accompanied with a district peak at 403 °C in the DTGA curve, corresponds to the oxidative decomposition of the organic part of 5-((3-(trimethoxysilyl)propyl)carbamoyl)-1H-imidazole-4-carboxylic acid. Moreover, this ~6.2% weight loss is corresponded to ~0.26 mmol/g loading of TMSIm on SBA-15. Furthermore, according to thermal analysis, the prepared compound is stable up to 403 °C.

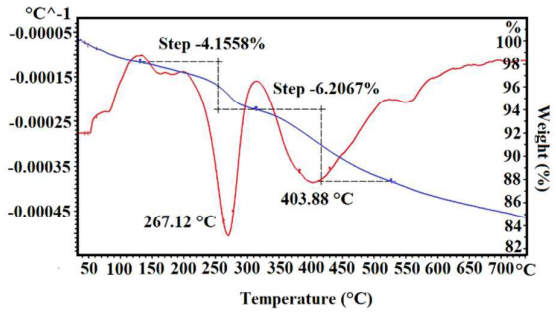

Figure 3 TGA/DTGA curves of [SBA-TMSIm].

Nitrogen adsorption/desorption isotherm and pore size distribution curve studies. Dinitrogen adsorption-desorption isotherms of SBA-15 and [SBA-15TMSIm] at 77 K are shown in Figure 4. A type IV profile with a type H1 hysteresis loop[34] which is characteristic of 1D cylindrical regular pores and capillary condensation were observed on the isotherms of both solids which is typical of mesoporous materials, according to IUPAC classification in the literature.[21,28,29,35-40] The pore size distribution curves of SBA-15 and [SBA-TMSIm] (Figure 5) obtained by the Barrett-Joyner-Halenda method shows narrow and uniform-sized mesopores with an average value of 4.6 nm for both solids.[21,35,36] The specific surface area (S_{BET}), estimated statitical thickness of adsorbed layer (2t) and pore volume (V_P) of SBA-15 and [SBA-TMSIm] are shown in Table 1. The BET

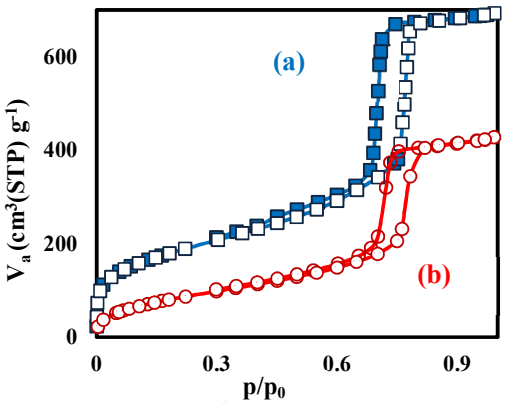

Figure 4 The nitrogen adsorption/desorption isotherms of (a) SBA-15 and (b) [SBA-TMSIm].

Table 1 Textural properties of SBA-15 and [SBA-TMSIm]

Solid	S_{BET}[a]/m^2 g^{-1}	2t[b]/nm	Vp[c]/cm^3 g^{-1}
SBA-15	551	3.6	1
[SBA-TMSIm]	347	7.8	0.66

[a] S_{BET} is the BET specific surface area.
[b] 2t is estimated statistical thickness of adsorbed layer.
[c] V_P is pore volume, obtained by BJH method.

View Article Online
DOI: 10.1039/C8NJ00743H
Journal Name ARTICLE

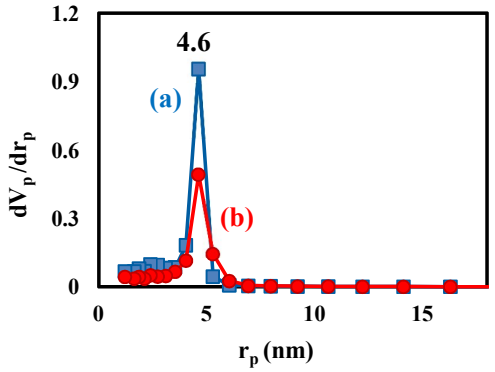

Figure 5 The pore size distribution curves by BJH method for (a) SBA-15 and (b) [SBA-TMSIm].

specific surface area and pore volume of the precursor mesoporous silica SBA-15 were of 551 m^2 g^{-1} and 1 cm^3 g^{-1}, respectively. The experimental data show that, at a given pressure, the thickness of the film increases upon decreasing the pore volume (V_p). As calculated from t-plot method, SBA-15 has a contribution of 20% of micropores. The values of micropore volume, microporous surface area and external surface area were of 1.03 cm^3 g^{-1},377 m^2 g^{-1}, and 581 m^2 g^{-1}, respectively. The covalent modification of SBA-15 with imidazole moieties to yield [SBA-TMSIm] was followed by a decrease in the BET specific surface area and pore volume to 347 m^2 g^{-1} and 0.66 cm^3 g^{-1}, respectively (Fig. 5a and b). These decreases can be explained by the presence of 5-((3-(trimethoxysilyl)propyl)carbamoyl)-1H-imidazole-4 carboxylic acid agent (TMSIm) that may block the access of N_2 gas to the SBA-15 pores or to the porous surface.[28,34,36,40,41] The values of micropore volume, microporous surface area and external surface area for [SBA-TMSIm] were of 0.61 cm^3 g^{-1},175 m^2 g^{-1}, and 398 m^2 g^{-1}. Microporous surface area and No changes in the diameter of the average pore (D_p) between SBA-15 and [SBA-15-TMSIm] were noticed, which is unlike to the data reported before.[37,41-43] This may be related to a much lower functionalization of [TMSIm] on SBA-15 (0.26 mmol g^{-1}) in compare to previous works.[28,35,41,43]

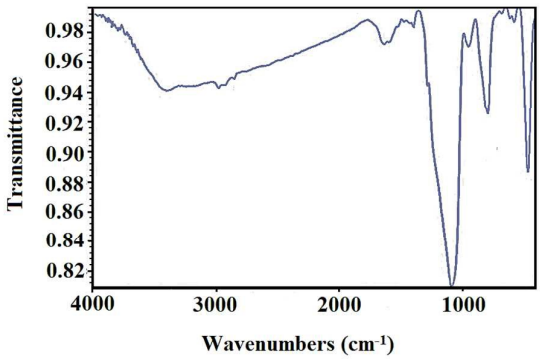

Figure 6 FTIR patterns of [Mn(TPP)OAc/SBA-TMSIm].

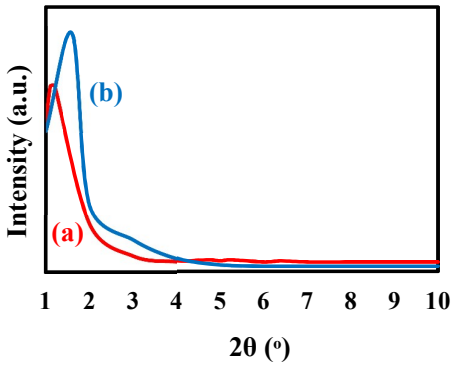

Figure 7 Low-angle XRD patterns of (a) [Mn(TPP)OAc/SBA-TMSIm] and (b) SBA-15.

Characterization of [Mn(TPP)OAc/SBA-TMSIm]

FT-IR spectra. Comparing the FT-IR spectra of functionalized [SBA-TMSIm] and [Mn(TPP)OAc/SBA-TMSIm] (Figure 6) reveals the appearance of C=C and C=N stretching bands of porphyrin at 1460-1650 cm^{-1} which confirms the attachment of manganese porphyrin to mesoporous silica support. The similarity between FT-IR spectra of functionalized porous materials and heterogenized catalysts indicates that the porous nature of the [SBA-TMSIm] has been kept after immobilizing the [Mn(TPP)OAc] onto them.

X-ray diffraction. Figure 7 shows the low-angle XRD pattern of [Mn(TPP)OAc/SBA-TMSIm] and SBA-15. Apparently, after functionalization of SBA-15 and grafting Mn(TPP)OAc, the intensity of diffraction peak decrease to some extent. This decrease can be attributed to the disordering of catalyst particles, and small shift to higher angle confirms the anchoring of porphyrin into SBA-15 cavities with preservation of the mesostructure.

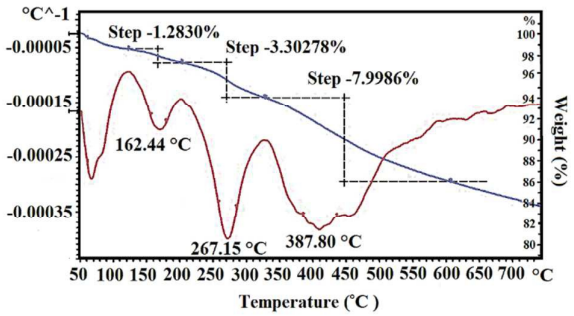

Figure 8 TGA/DTGA curves of [Mn(TPP)OAc/SBA-TMSIm].

TGA/DTGA analysis. Thermogravimetric analysis of [Mn(TPP)OAc/SBA-TMSIm] exhibits the thermal behaviour of the final heterogeneous catalyst (Figure 8). Four weight loss events took place in the TGA/DTGA diagram. The first event at 162 °C with about 1.2% weight loss is related to the physical

View Article Online
DOI: 10.1039/C8NJ00743H

desorption of the water molecules in the [Mn(TPP)OAc/SBA-TMSIm]. The second step is associated with the loss of free water molecules, which are inside cylindrical pores, or water molecules that established a link through hydrogen bonding with SiO_2 and released at 267 °C as mentioned before. Finally, the mass decline around 387 °C can be attributed to the decomposition of [Mn(TPP)OAc] and the (TMSIm) agent together.

Nitrogen adsorption/desorption isotherm and pore size distribution studies. Dinitrogen adsorption-desorption isotherms of [Mn(TPP)OAc/SBA-TMSIm] at 77 K are shown in Figure 9. Once more, a type IV profile with a type H1 hysteresis loop observed for this catalyst similar to the modified SBA-15.[34] The pore size distribution curves of [Mn(TPP)OAc/SBA-TMSIm] (Figure 10) shows narrow and uniform-sized mesopores with an average value of 4.6 nm similar to the solid support. The BET

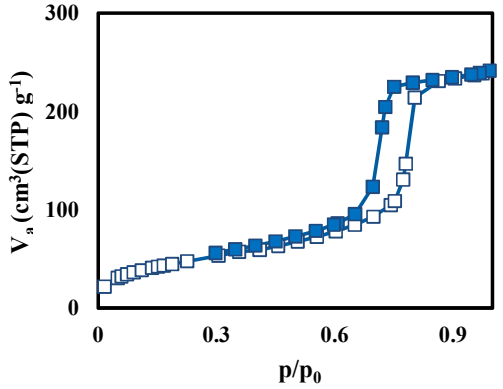

Figure 9 The nitrogen adsorption/desorption isotherms of [Mn(TPP)OAc/SBA-TMSIm].

Table 2 Textural properties of [Mn(TPP)OAc/SBA-TMSIm]

Solid	S_{BET}/m^2 g^{-1}	2t/nm	V_p/cm^3 g^{-1}
[Mn(TPP)OAc/SBA-TMSIm]	170	6.1	0.37

[a] S_{BET} is the BET specific surface area.
[b] 2t is estimated statistical thickness of adsorbed layer.
[c] V_P is pore volume, obtained by BJH method.

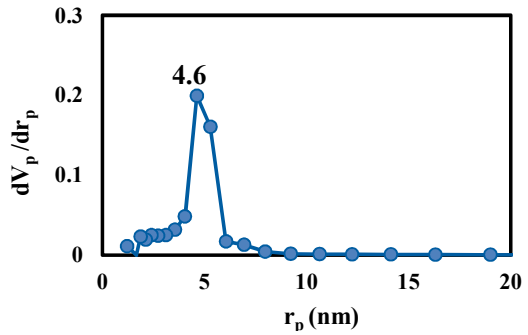

Figure 10 The pore size distribution curves by BJH method for [Mn(TPP)OAc/SBA-TMSIm].

specific surface area along with the texture of [Mn(TPP)OAc/SBA-TMSIm] are listed in Table 2. The values of micropore volume, microporous surface area and external

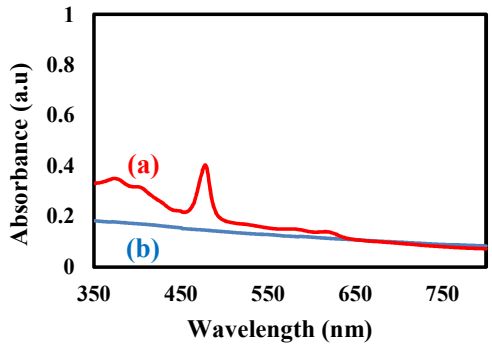

Figure 11 UV-Vis absorption spectra of (a) [Mn(TPP)OAc/SBA-TMSIm] and (b) [SBA-TMSIm] in dichloromethane.

surface area were of 0.34 cm^3 g^{-1},79 m^2 g^{-1}, and 122 m^2 g^{-1}, respectively. As expected, a decrease in the BET specific surface area and pore volume in comparison to the SBA-15 is clear.

UV-Vis spectroscopy. The presence of Mn-porphyrin in the functionalized SBA-15 was also confirmed by UV–Vis spectroscopy (Figure 11). No absorption band was observed in the UV–Vis spectrum of [SBA-TMSIm] [Figure 11(b), dash line]. However, the Soret band at 480 nm and Q bands at 583 and 622 nm appear after anchoring of [Mn(TPP)OAc] into cylindrical pores of [SBA-TMSIm] [Figure 11(a)].

nm appear after anchoring of [Mn(TPP)OAc] into cylindrical pores of [SBA-TMSIm] [Figure 11(a)].

Atomic absorption spectroscopy (AAS). The manganese content of heterogeneous catalyst was measured by atomic absorption spectroscopy. Based on this analysis, the Mn content of the catalyst is about 120 µmol/g (87 mg of [Mn(TPP)OAc] per 1 g).

Catalytic studies

Styrene is a standard substrate for studying the catalytic performance for the homolytic activation of C=C in alkene oxidation, and for estimating yield selectivity toward styrene oxide with respect to further oxidation products. Moreover, styrene oxide is an essential organic intermediate.[44,45] Therefore, the quest for discovering systems that are capable of catalyzing styrene and other alkenes under mild conditions still stands a challenge for academic researchers.

The heterogenized manganese porphyrin [Mn(TPP)OAc/SBA-TMSIm] was evaluated as a catalyst for styrene oxidation using molecular oxygen as a green oxidant and isobutyraldehyde (IBA) as a co-reducer. We performed a blank experiment with 30 mmol styrene and 90 mmol of isobutyraldehyde in acetonitrile at 50 °C, which afforded styrene oxide (3%) after 1 h according

DOI: 10.1039/C8NJ00743H

Table 3 Effect of time and temperature in oxidation of styrene with molecular oxygen catalyzed by [Mn(TPP)OAc/SBA-TMSIm] in acetonitrile

Entry	Temp. (°C)	Time (h)	Conv. (%)	Yeild (%)	
				Benzaldehyde	Epoxy styrene
1	25	4	3	3	-
2	25	5	12	7	5
3	25	6	20	10	10
4	25	7	31	17	14
5	25	24	70	41	29
6	40	1	27	11	16
7	40	2	80	30	50
8	50	1	90	21	69

[a]The reaction conditions are as follows: 0.0021 mmol of catalyst, 0.0189 mmol of styrene, 0.0567 mmol of isobutyraldehyde.

to GC analysis. However, the addition of a catalytic amount of [Mn(TPP)OAc/SBA-TMSIm] (0.0021 mmol) to the acetonitrile mixture led to 90% conversion of styrene to styrene oxide or benzaldehyde under the same conditions.

In order to optimize the reaction conditions, the effect of reaction time and temperature on the oxidation of styrene was investigated. It is observed that the highest conversion of styrene (70%) was obtained after 24 h at 25 °C (Table 3, entry 5) while at 50 °C after 1 h 90 % conversion of styrene was obtained (Table 3, entry 8). In addition, it is observed that product selectivity is dependence to the reaction temperature. At the room temperature, benzaldehyde is the major product while at 50 °C epoxy styrene is the major product.

Homogeneous oxidation of styrene with molecular oxygen in the presence of Mn(TPP)OAc and in the same conditions, led to process not only did not cause catalyst deactivation but also improve the catalytic performance.

Having proved the activity and stability of [Mn(TPP)OAc/SBA-TMSIm] in the model reaction, the scope of the protocol was subsequently extended to a range of olefins, as shown in Figure 12. In this catalytic system, the oxidation of cyclooctene (59%), 4-methoxy styrene (81%) and cis-stilbene (40%) give the corresponding epoxide as the sole product at 50 °C after 1 h.

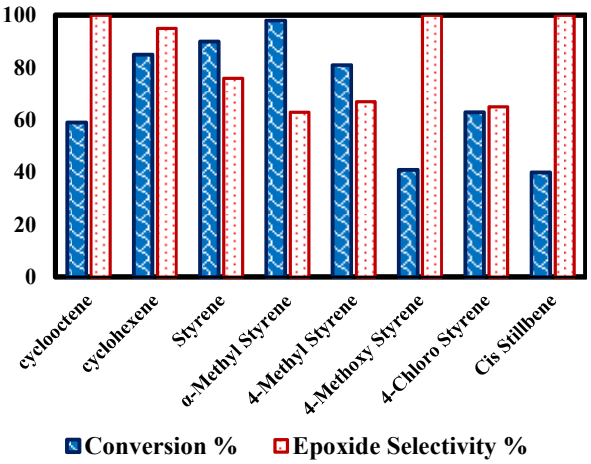

Figure 12 Epoxidation of various olefins using O_2/IBA as oxidant, catalyzed by [Mn(TPP)OAc/SBA-TMSIm] in CH_3CN at 50 °C temperature.

Proposed mechanism

The mechanism for the metalloporphyrin-catalyzed aerobic oxidation of olefins such as styrene in the presence of isobutyraldehyde generally involves a free radical process and isobutyraldehye is a common reducing agent.[46] In the proposed Mechanism (Scheme 2), two pathways could be occurred.[47] (i) Mn(III)(TPP) reacts with the aldehyde to generate an acyl radical (a) and Mn(II)(TPP) (pathway I in scheme 2) and then the acyl radical react with molecular oxygen to generate acylperoxy radical (b) which is capable for the oxidation of alkenes. (ii) Mn(II)(TPP) reacted with peroxy acid (c), which is generated

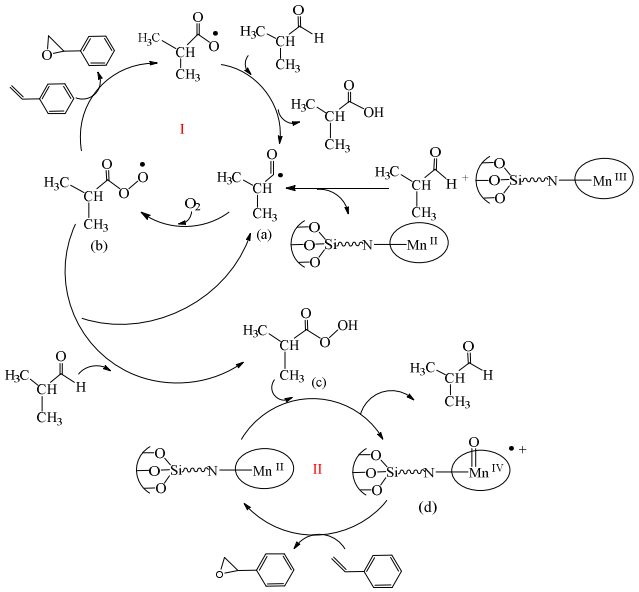

Scheme 2 Plausible mechanism of styrene oxidation catalyzed by Mn(III) porphyrin in the presence of molecular oxygen and isobutyraldehyde.

from the reaction of (b) with another aldehyde molecule, to generate high-valent Mn(IV) porphyrin(d) (pathway II in scheme 2) which has a high oxidizing power to form the oxidation products.

Conclusions

In summary, new and efficient mesoporous imidazole-functionalized SBA-15 were synthesized and characterized and its use as support for immobilization of [Mn(TPP)OAc] within axial coordination was discussed. The heterogeneous catalyst [Mn(TPP)OAc/SBA-TMSIm] is a well-organized system for oxidation of olefins with high conversion yields and nice selectivity. Molecular oxygen balloon was used as an environmentally friendly oxidant in the reactions and due to its inert triplet system, isobutyraldehyde was utilized as an activator for the oxidant.

View Article Online
DOI: 10.1039/C8NJ00743H

Conflicts of interest

"There are no conflicts to declare".

Acknowledgements

Financial support of this work by K.N. Toosi University of Technology Research Council and Iran National Science Foundation (INSF) under grant No. 96005913 is acknowledged.

References

1 H. B. Ji and X. T. Zhou, *Biomimetics Learning from Nature*, ed. A. Mukherjee, Vukovar, Croatia, 2010.
2 D. J. C. Constable, P. J. Dunn, J. D. Hayler, G. R. Humphrey, J. L. Leazer, R. J. Linderman, K. Lorenz, J. Manley, B. A. Pearlman, A. Wells, A. Zaks, and T. Y. Zhang, *Green Chem.*, 2007, **9**, 411-420.
3 C. Parmeggiani, and F. Cardona, *Green Chem.*, 2012, **14**, 547-564.
4 X. T. Zhou, H. B. Ji, H. C. Xu, H. L. X. Pei, L. F. Wang and X. D. Yao, *Tetrahedron Lett.*, 2007, **48**, 2691-2695.
5 S. Sahu, and D. P. Goldberg, *J. Am. Chem. Soc.*, 2016, **138**, 11410-11428.
6 H. M. Neu, J. Jung, R. A. Baglia, M. A. Siegler, K. Ohkubo, S. Fukuzumi, and D. P. Goldberg, *J. Am. Chem. Soc.*, 2015, **137**, 4614-4617.
7 B. Fu, H. C. Yu, J. W. Huang, P. Zhao, J. Liu, L. N. Ji, *Journal of Molecular Catalysis A: Chemical*, 2009, **298**, 74-80.
8 Y. Fei. Li, C. C. Guo, X. H. Yan, and Q. Liu, *J. Porphyrins Phthalocyanines*, 2006, **10**, 942-947.
9 T. L. Poulos, *Chem. Rev.*, 2014, **114**, 3919-3962.
10 R. A. Baglia, J. P. T. Zaragoza, and D. P. Goldberg, *Chem. Rev.* 2017, **117**, 13320-13352.
11 S. Rayati a, S. Zakavi, V. Noroozi, S. H. Motlagh, *Catalysis Communications*, 2008, **10**, 221-226.
12 O. Pouralimardan, A. C. Chamayou, C. Janiak, H. Hosseini-Monfared, Inorg. Chim. Acta, 2007, **360**, 1599-1608.
13 M. Ghorbanloo, H. Hosseini-Monfared, C. Janiak, *J. Mol. Catal. A: Chem.* 2011, **345**, 12-20.
14 S. Nakagaki, K. M. Mantovani, G. S. Machado, K. A. D. F. Castro, and F. Wypych, *Molecules*, 2016, **21**, 291.
15 E. Brule, and Y. R. Miguel, *Org. Biomol. Chem.*, 2006, **4**, 599-609.
16 G. Huang, R. X. Yuan, Y. Peng, X. F. Chen, S. K. Zhao, S. J. Wei, W. X. Guo, and X. Chen, *RSC Adv.*, 2016, **6**, 48571-48579.
17 H. Ebrahimzadeh, A. A. Asgharinezhad, N. Tavassoli, O. Sadeghi, M. M. Amini, and F. Kamarei, *Intern. J. Environ. Anal. Chem.* 2012, **92**, 509-521.
18 W. J. J. Stevens, K. Lebeau, M. Mertens, G. van Tendeloo, P. Cool, and E. F. Vansant, *J. Phys.Chem. B*, 2006, **110**, 9183-9187.
19 F. Zhang, Y. Yan, H. Yang, Y. Meng, C. Yu, B. Tu, D. Zhao, *J. Phys. Chem*. 2005, **109**, 8723-8732.
20 N. Rahmat, A. A. Zuhairi, A. Rahman Mohamed, *Am. J. Appl. Sci.* 2010, **7**, 1579-1586.
21 F. J. V. E. Oliveira, M. A. Melo Jr., C. Airoldi, *Mater. Res. Bull.*, 2013, **48**, 1045-1056.
22 I. Sierra, D. Pérez-Quintanilla, Chem. Soc. Rev. 2013, **42**, 3792-3807.
23 J. A. Melero, G. Morales, J. Iglesias, M. Paniagua, B. Hernández, S. Penedo, *Appl. Catal. A Gen.* 2013, **466**, 116-122.
24 F. Hoffmann, M. Cornelius, J. Morell, M. Fröba, *Angew. Chem.* Int. Ed. 2006, **45**, 3216-3251.
25 D. Adler, F. R. Longo, J. D. Finarelli, J. Golldmacher, J. Assour, L. Korsakoff, *J. Org. Chem.*, 1976, **32**, 476-476.
26 J. W. Buchler, G. Eikellmann, J. Puppe, K. Rohback, H. Schneehage, and D. Weck *Justus Liebigs Ann.Chem.* 1971, **745**, 135-151.
27 X. Shi, B. Fan, H. Li, R. Li, W. Fan, *Micropor. Mesopor. Mater.*, 2014, **196**, 277-283.
28 S. Alavi, H. Hosseini-Monfared, M. Siczek, *J. Mol. Catal. A Chem.*, 2013, **377**, 16-28.
29 S. Hashemikia, N. Hemmatinejad, E. Ahmadi, M. Montazer, *J. Colloid Interface Sci.*, 2015, **443**, 105-114.
30 R. Tayebee, M. M. Amini, M. Akbari, and A. Aliakbari, *Dalton Trans.*, 2015, **44**, 9596-9609.
31 R. Tayebee, M. M. Amini, S. Pouyamanesh, and A. Aliakbari, *Dalton Trans.*, 2015, **44**, 5888-5897.
32 M. Behbahani, A. A. Akbari, M. M. Amini, and A. Bagheri, *Anal. Methods*, 2014, **6**, 8785-8792.
33 J. Li, L. Wang, T. Qi, Y. Zhou, C. Liu, J. Chu, and Y. Zhang, *Micropor. Mesopor. Mater.,* 2008, **110**, 442-450.
34 M. Thommes, K. Kaneko, A. V. Neimark, J. P. Olivier, F. Rodriguez-Reinoso, J. Rouquerol, and K. S. W. Sing, *Pure Appl. Chem.,* 2015, **87**, 1051-1069.
35 Q. Zhu, S. Maeno, R. Nishimoto, T. Miyamoto, M. Fukushima, *J. Mol. Catal. A Chem.*, 2014, **385**, 31-37.
36 D. Zhao, J. Feng, Q. Huo, N. Melosh, G. H. Fredrickson, B. F. Chmelka, G. D. Stucky, *Science*, 1998, **279**, 548-552.
37 E. Sujandi, E. A. Prasetyanto, S. C. Lee, S. E. Park, *Micropor. Mesopor. Mater*., 2009, **118**, 134-142.
38 D. Zhao, J. Sun, Q. Li, G.D. Stucky, *Chem. Mater*., 2000, **12**, 275-279.
39 S. M. L. Santos, K. A. B. Nogueira, M. S. Gama, J. D. F. Lima, I. J. Silva, D. C. S. Azevedo, *Micropor. Mesopor. Mater*., 2013, **180**, 284-292.
40 M. J. Nasab, A. R. Kiasat, *RSC Adv*., 2015, **5**, 75491-75499.
41 J. Q. Wang, L. Huang, M. Xue, Y. Wang, L. Gao, J. H. Zhu, Z. Zou, *J. Phys. Chem. C.*, 2008, **112**, 5014-5022.
42 M. J. Nasab, A. R. Kiasat, *RSC Adv*., 2015, **5**, 75491–75499.
43 A. Schlossbauer, D. Schaffert, J. Kecht, E. Wagner, T. Bein, *J. Am. Chem. Soc*., 2008, **130**, 12558-12559.
44 M. Selvaraj, S.W. Song, S. Kawi, *Micropor. Mesopor. Mater.*, 2008, **110**, 472-479.
45 B. Tyagi, B. Shaik, and H. C. Bajaj, *Appl. Catal. A: General*, 2010, **383**, 161-168.
46 Yu. Rongbing, S. Zhang, Y. Luo, R. Bai, J. Zhou, H. Song, *New J. Chem.*, 2015, **39**, 5096-5099.
47 H. B. Ji, X. T. Zhou. Biomimetic Epoxidation of Olefins Catalyzed by Metalloporphyrins with Molecular Oxygen; INTECH Open Access Publisher, 2011.

View Article Online
DOI: 10.1039/C8NJ00743H

Graphical abstract